



Numerical simulation-aided particle filter-based damage prognosis using Lamb waves

Tianzhi Li^a, Luca Lomazzi^a, Francesco Cadini^a, Claudio Sbarufatti^a, Jian Chen^b, Shenfang Yuan^b

^a Dipartimento di Meccanica, Politecnico di Milano, Milan, Italy

^b Research Center of Structural Health Monitoring and Prognosis, State Key Laboratory of Mechanics and Control of Mechanical Structures, Nanjing University of Aeronautics and Astronautics, Nanjing, China

ARTICLE INFO

Communicated by Wieslaw Ostachowicz

Keywords:

Structural health monitoring
Damage prognosis
Numerical simulation
Particle filter
Lamb wave

ABSTRACT

Damage prognosis generally resorts to a damage evolution model and the current damage state to predict the future state and the remaining useful life (RUL). As a properly defined damage-sensitive statistical feature extracted from the Lamb waves can be used to online quantify the damage state, it is here exploited within a particle filter (PF) scheme to perform damage prognosis in structural health monitoring. An accurate mapping between the damage state and this feature would require a sufficient set of experimental Lamb waves collected in correspondence of different damage levels occurring during the run-to-failure process, which, however, is not usually available in real practice due to the high costs and the complex logistics involved in such experimental campaigns. In order to deal with this issue, this paper develops a new numerical simulation-aided particle filter-based damage prognosis framework, where the process equation is still built on the basis of available physical knowledge about the degradation process, whereas the measurement equation is built by means of a data-driven modeling approach using the features extracted from the numerically simulated Lamb waves. The PF framework serves as the state estimation tool which allows to identify the damage state and the parameters in the two equations. The future damage states and the RUL can finally be predicted by projecting the PF estimates in the future using the process equation. The proposed framework is demonstrated with reference to experimental studies of fatigue crack growth in aluminum lug structures with online Lamb wave monitoring.

1. Introduction

Engineering structures have to withstand various mechanical and environmental loads during their service life, resulting in fatigue damage, e.g., a crack in a metallic structure or a delamination in a composite. The damage may usually evolve in time (or load cycles in structural fatigue problems), so that, eventually, the structure fails when the damage state reaches a pre-defined threshold, beyond which its functionality cannot be guaranteed any longer. In order to timely avoid this issue, usually inspections are carried out to evaluate the structural performance, often requiring quite high financial expenses, also due to unwanted system shutdowns. In order to simultaneously ensure structural safety and reduce maintenance costs, one possibility is to schedule the maintenance just before the damage state reaches the critical limit. In this context, an advanced damage prognosis technique is desired to estimate the time

E-mail address: francesco.cadini@polimi.it (F. Cadini).

<https://doi.org/10.1016/j.ymssp.2022.109326>

Received 10 November 2021; Received in revised form 24 February 2022; Accepted 17 May 2022

Available online 30 May 2022

0888-3270/© 2022 The Authors. Published by Elsevier Ltd. This is an open access article under the CC BY license (<http://creativecommons.org/licenses/by/4.0/>).

required by the state to become not reach the threshold value, i.e., the structure remaining useful life (RUL).

As the damage evolution under a certain service condition may follow a specific pattern, the future state can be calculated by the current one by means of a proper model describing such a pattern. These damage evolution models in prognostic practices can be either physics-based [1–3] or data-driven [4–6], according to the type of information used for modeling the damage behavior, namely the physical knowledge or observed data, respectively. Physics-based models utilize the physical knowledge, such as Paris' law [1] and its extensions [2,3], to relate the damage state with the load cycles and external loading conditions, while data-driven models, e.g., neural network [4] and non-homogenous hidden semi Markov model [5,6], resort to sufficient monitoring data collected during the degradation process for depicting the above relationship. There are no universally best models, given that each type of model has its own advantages and disadvantages [7,8].

On the other hand, no matter which type of model is adopted, any deterministic form of a damage evolution model can hardly provide an accurate prognostic result, given the uncertainties arising from complex structural degradations [9], the environmental effects [10], and the sensor health conditions [10]. A common strategy for these models to improve their prognostic performances is to set the model parameters as unknown variables to be updated online by a state estimation technique, such as particle filter (PF), given its demonstrated performances in nonlinear and non-Gaussian problems.

Another issue in RUL prediction is the required quantification of the current damage state through a direct or indirect measurement system. The first approach, i.e., when the damage state can be directly measured, has already received plenty of investigations in this field, such as for example the case of the crack length in a metallic structure acquired by a caliper [1,4] or that of matrix cracking density and delamination length in composites measured by X-rays [2,3]. In case the damage state cannot be directly measured, one may refer to an indirect measurement system, such as fiber Bragg grating strain sensors [11] or Lamb wave-based monitoring systems [12–14], to infer the damage state through a measurement equation describing the relationship between the damage state and the measurement (either the directly measured signal or some statistical feature extracted from the signal). Such equation is usually built through a data-driven modeling technique, e.g., neural network [11], polynomial function [14], leave-one-out method [13] or Gaussian process regression [12].

Among the available sensing systems for SHM applications, those based on Lamb waves are probably the most promising, due to their capability for online operation and high sensitivity to damage [15]. Their efficiency in prognostic investigations has been well demonstrated in several works, e.g., [12–14], where an accurate mapping between the damage state and the feature extracted from the Lamb waves requires a sufficiently large database of signals during the run-to-failure process, which, unfortunately, rarely occurs, mainly due to too high costs. On the other hand, numerical Lamb wave simulations can capture the actual Lamb wave propagation, possibly leading to a satisfactory agreement between the features extracted from the numerical Lamb waves and those from the experimental signals. This allows adopting the numerical features taken at different damage state levels, e.g., crack lengths in metal [16,17] or delamination sizes in composite [18], to empirically build the measurement equation following the procedure indicated above. However, this method has not been used for damage prognosis so far, which might be because the unavoidable bias between the features predicted by the measurement equation and those obtained from the experimental Lamb waves [16,18] can lead to severely inaccurate online prognostic results, as already discussed in [14].

By combining the numerical simulation-aided damage quantification method [16–18] with a damage prognosis approach accounting for the measurement bias [14], this paper proposes a novel numerical simulation-aided particle filter-based damage prognosis framework, where the numerical Lamb waves are used to build the measurement equation. The proposed framework consists of four main steps. First, the numerical Lamb wave simulations of the monitored structure are developed to provide the statistical features of the Lamb waves at different damage levels (or extents). Second, the process equation is formulated using both a bias parameter and the physical law describing damage propagation, whereas the measurement equation representing the relationship between the damage state and the observed feature is built by resorting to a data-driven technique and the use of a bias parameter. Third, a PF is used to estimate the damage state, the damage parameters, and the bias. Finally, the future states and the RUL can be estimated by

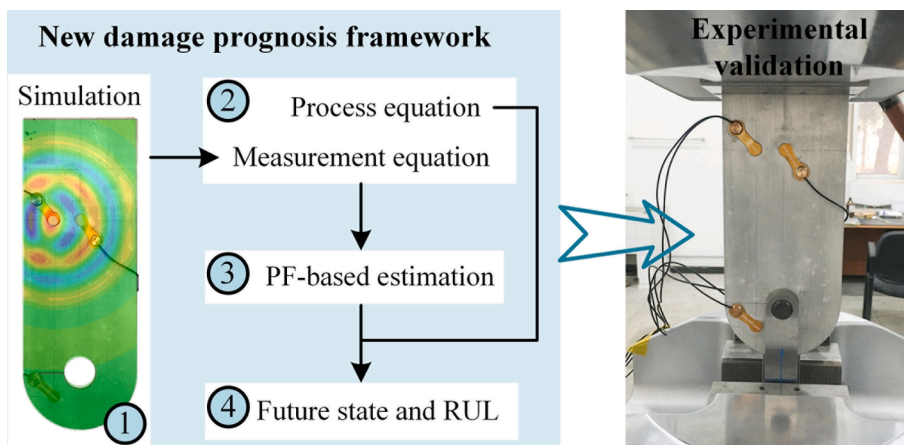


Fig. 1. Numerical simulation-aided PF-based damage prognosis framework.

projecting into the future the process equation starting from the current PF-based estimates of the damage state. The proposed prognosis framework is demonstrated by an experimental study, where an aluminum lug structure subject to fatigue crack growth (FCG) is monitored by a Lamb wave measurement system.

The rest of this paper is organized as follows: Section 2 introduces the four main steps in the prognosis framework. The numerical and experimental Lamb waves are discussed in Section 3, while the application of the proposed method to the experimental case study is provided in Section 4. Finally, Section 5 concludes this paper.

2. Novel damage prognosis framework

Fig. 1 presents the four main steps of the proposed damage prognosis framework, namely, (i) simulating the Lamb waves at different damage levels by means of the numerical model, (ii) formulating a state space model, (iii) estimating the damage state, its damage evolution model parameters, and the bias by PF, and (iv) projecting into the future by the process equation starting from the current PF estimates. The main novelty of the proposed prognosis framework compared to the state-of-the-art methods [12–14] is that numerical Lamb waves at different damage levels, instead of experimental signals, are used for formulating a measurement equation, so that the costs and efforts in conducting run-to-failure tests or collecting in-field data for model formulation can be avoided. The four steps of the proposed procedure are introduced below, and the experimental setup and validation will be discussed in Sections 3 and 4, respectively.

2.1. Lamb wave simulation

Depending on the type of excitation used in a numerical model, the Lamb wave simulations can be broadly divided into two categories, i.e., (i) those using voltage [18,19] and (ii) those using mechanical loads like force [16], pressure [20], or displacement [17]. The first ones are similar to how the actuator and sensor work in a real experiment. The actuator and sensor are modeled as elements with electro-mechanical and mechanical properties. The former can deform when receiving the voltage and consequently lead to the vibration of the monitored structure to which it is attached, while the latter one deforms with the vibration and consequently generates the voltages, which are taken as the numerical Lamb wave.

As to the second type of simulations, the modeling for the actuator and sensor is not mandatory. The excitation at the actuator location can be a mechanical load like force [16], pressure [20], or displacement [17], while the vibration responses at the sensor location, e.g., out-of-the plane displacement, are taken as the numerical Lamb wave. These simulations can provide three modes of Lamb waves, i.e., full mode, pure *S* mode, and pure *A* mode, corresponding to one single excitation, two symmetric excitations, and two anti-symmetric excitations. Note that many numerical models [16–19] will only have either S_0 , A_0 or both two modes simulated by applying an excitation with a relatively small center frequency. High-order Lamb waves may not be frequently used in SHM practices.

As the two types of numerical simulations can capture the actual Lamb wave propagation, some statistical features calculated from numerical Lamb waves are in good agreement with those from experimental ones, which enables the feasibility of adopting the numerical features to formulate a measurement equation for damage quantification, as already performed in [16–18]. In this study, the Lamb wave simulations of the monitored structure are conducted to provide the features at different levels of damage, which will be then adopted to formulate a measurement equation, as will be introduced in Section 3.

2.2. Prognostic model

In general, upon proper discretization in time (or load cycle), the damage evolution can be described by:

$$x_k = f(x_{k-1}, \theta) \quad (1)$$

where x is the damage state, $f(\cdot)$ is the evolution function, θ is a model parameter vector, and the subscript k is the discrete time step index. Due to the uncertainties in the damage evolution process, the parameters θ can vary in different specimens of the same structure. According to the common practice of PF-based diagnosis and prognosis, the unknown parameters are treated as stochastic variables (similarly to the damage state) that can be added to the state vector [13,14],

$$\begin{bmatrix} \theta_k \\ x_k \end{bmatrix} = \begin{bmatrix} \theta_{k-1} + \omega_{\theta,k} \\ f(x_{k-1}, \theta_k, \omega_k) \end{bmatrix} \quad (2)$$

where ω_k and ω_{θ} are the process noises for the damage state and the parameters, respectively, accounting for their stochasticity.

With a proper measurement y (i.e., a feature extracted from the Lamb waves in this study) for inferring the unknown damage state, the measurement equation in a PF-based damage prognosis can be formulated as:

$$y_k = g(x_k) + \nu_k \quad (3)$$

where the function $g(\cdot)$ describes the relationship between the damage state and the measurement, ν_k is the measurement noise assumed as zero-mean Gaussian distributed. Current PF and Lamb wave-based damage prognosis practices [13,14] usually resort to the Paris' law, or an extension thereof, and a data-driven model to describe the damage state process evolution $f(\cdot)$ and to approximate the relationship $g(\cdot)$, respectively, with the latter usually requiring the availability of a sufficiently large training dataset during the run-to-

failure process of a structure.

Given the difficulties and costs associated with the acquisition of sufficiently informative datasets in laboratory experiments or, even, in the field, some Lamb wave-based damage quantification investigations [16–18] have adopted the features from numerically simulated Lamb waves to build the function $g(\cdot)$. However, the unavoidable biases between the features predicted by $g(\cdot)$ and those extracted from experimental Lamb waves acquired on a testing specimen may not lead to satisfactory prognostic results, as already discussed in [14].

By combining the numerical simulation-aided damage quantification method in [16–18] with the approach to damage prognosis in presence of significant measurement bias [14], this paper develops a novel prognosis framework that resorts to the numerical Lamb waves for building the measurement equation, where the effect of the unavoidable bias can be alleviated by further augmenting the state space with a bias parameter for estimation. The prognostic framework finally reads,

$$\begin{cases} \mathbf{z}_k = \begin{bmatrix} \boldsymbol{\theta}_k \\ x_k \\ b_k \end{bmatrix} = \begin{bmatrix} \boldsymbol{\theta}_{k-1} + \boldsymbol{\omega}_{\boldsymbol{\theta},k} \\ f(x_{k-1}, \boldsymbol{\theta}_k, \omega_k) \\ b_{k-1} + \omega_{b,k} \end{bmatrix} \\ y_k = g(x_k) + b_k + \nu_k \end{cases} \quad (4)$$

where b is the bias parameter and ω_b is its associated process noise, and \mathbf{z}_k is a newly defined augmented state vector including both the state and the parameters to be estimated,

2.3. Particle filter

In a Bayesian approach, the unknown state vector at k -th step \mathbf{z}_k can be inferred from the measurement as:

$$p(\mathbf{z}_k | \mathbf{y}_{1:k-1}) = \int p(\mathbf{z}_k | \mathbf{z}_{k-1}) p(\mathbf{z}_{k-1} | \mathbf{y}_{1:k-1}) d\mathbf{z}_{k-1} \quad (5)$$

$$p(\mathbf{z}_k | \mathbf{y}_{1:k}) \propto p(y_k | \mathbf{z}_k) p(\mathbf{z}_k | \mathbf{y}_{1:k-1}) \quad (6)$$

where $\mathbf{y}_{1:k}$ is the measurement vector collected from time step 1 to k , the symbol \propto means ‘proportional to’, the transition distribution $p(\mathbf{z}_k | \mathbf{z}_{k-1})$ and the likelihood function $p(y_k | \mathbf{z}_k)$ denote the process and measurement equations, respectively, $p(\mathbf{z}_k | \mathbf{y}_{1:k-1})$ and $p(\mathbf{z}_k | \mathbf{y}_{1:k})$ are the prior and posterior probability distribution function (PDF), respectively.

Eqs. (5) and (6) form the basis for the optimal Bayesian solution, which is, however, difficult to be analytically calculated in a nonlinear and non-Gaussian system like Eq. (4). Therefore, the sampling importance resampling (SIR) PF [21], as an efficient state estimation in this kind of problem, is used in this study. Table 1 lists the pseudo-code of the SIR PF.

2.4. Prediction for future state and RUL

Within the PF framework, by resorting to the damage evolution model of Eq. (1) and the k -th posterior PDF of damage state $p(x_k | \mathbf{y}_{1:k})$, the prognostic stage enables the prediction of the q -th step ahead posterior PDF of the damage state $p(x_{k+q} | \mathbf{y}_{1:k})$ as [22]:

$$p(x_{k+q} | \mathbf{y}_{1:k}) = \int \cdots \int \prod_{j=k+1}^{k+q} p(x_j | x_{j-1}) p(x_k | \mathbf{y}_{1:k}) \prod_{j=k}^{k+q-1} dx_j \quad (7)$$

where $p(x_j | x_{j-1})$ is the so-called prior distribution, directly associated to the process equation.

Given the difficulty in analytically calculating the solution of Eq. (7), one alternative within a PF-based prognosis framework is to approximate the PDF by the particles and their weights as [23]:

Table 1
Sampling importance resampling particle filter.

Initialization: draw N_p particles $\{z_0^i : i = 1, 2, \dots, N_p\}$ from the initial distribution $p(z_0)$

For $k = 1, 2, \dots$,

Prediction in PF: draw N_p particles $\{z_k^i : i = 1, 2, \dots, N_p\}$ by $z_k^i \sim p(z_k | z_{k-1}^i)$

Weight update: calculate the weight w_k^i by $w_k^i \propto p(y_k | z_k^i)$, and then assign its normalized form \tilde{w}_k^i to each particle z_k^i

Resample for $\{z_k^i : i = 1, 2, \dots, N_p\}$ using the particle weights $\{\tilde{w}_k^i : i = 1, 2, \dots, N_p\}$

Approximate the estimate \hat{z}_k from $\hat{z}_k = \frac{1}{N_p} \sum_{i=1}^{N_p} z_k^i$

End

$$p(x_{k+q}|y_{1:k}) = \sum_{i=1}^{N_p} \tilde{w}_{k+q-1}^i p(x_{k+q}|x_{k+q-1}^i) \quad (8)$$

where \tilde{w}_{k+q-1}^i is the weight of the i -th particle at time step $k+q-1$, considered independent from q and equal to $1/N_p$ as the q -step ahead particle projection is done after resampling at each iteration in this study, whereas $p(x_{k+q}|x_{k+q-1}^i)$ can be computed through Eq. (1) and the PF state estimates available at the k -th step.

Table 2 summarizes the calculation required to obtain the estimate of the posterior of the future state and the RUL. The RUL prediction generally requires the definition of an additional threshold value of the damage state l_{th} . The structure is considered to fail when the future state calculated through Eq. (1) reaches the threshold, so that the RUL turns out to be equal to the multiplication of the number of prediction steps and the number of load cycles ΔN in one step.

3. Experimental and numerical Lamb waves

The experimental setup and the physical behavior of the Lamb waves are briefly introduced in Sections 3.1 and 3.2, respectively. The numerical models of the Lamb waves generated and propagating within the experimental specimen are developed in Section 3.3. Section 3.4 compares the Lamb waves from the two studies, which are then adopted to provide some features for damage quantification in Section 3.5.

3.1. Experimental setup

Fatigue tests of the lug joint aluminum structure equipped with a Lamb wave-based monitoring system [13,24], as given in Fig. 2 (a) and (b), are used to validate the proposed method. The thickness of the specimen and the diameter of the through hole are 5 mm and 25 mm, respectively. One 2 mm long notch is machined at the edge of the hole to initiate the crack growth. The MTS810 electro-hydraulic servo material test system is employed to provide the sinusoidal tensile fatigue load. The maximum load L_{max} , load ratio R , and loading frequency are 18 kN, 0.1, and 10 Hz, respectively.

Fig. 2 (c) presents the crack and the scale lines on the surface observed by a digital microscope. These lines are equally spaced by 1 mm. The fatigue loading is occasionally paused during the test, and an 18 kN static tensile load is applied to the structure to open the crack for better visualization. The crack length is considered to increase by 1 mm once the crack tip reaches the next line. A pre-cracking step is performed at the beginning of the fatigue test until the crack length reaches 3 mm.

Fig. 3 shows the crack growths observed for the five specimens S1 ~ S5 under fatigue testing. Due to the uncertainties from the material property, specimen assembling, external loading condition, etc., an obvious dispersion can be noted among the propagation trajectories of these specimens, which confirms that a deterministic damage evolution model can hardly provide accurate prognostic results. Similarly to [12], a 3 mm crack is taken as the initial crack, and the maximum crack length 22 mm is set as the threshold for damage prognosis.

As shown in Fig. 2 (b), the two piezoelectric transducers for crack monitoring are bonded on the surface of the structure with epoxy resin, and they are working with d_{31} mode. At each measured crack length, i.e., when the 18 kN static tensile load is applied to the structure, one serves as the actuator providing a 3-cycles Hanning-windowed sine burst with the central frequency 160 kHz, and another one serves as the sensor collecting the Lamb wave with a sampling frequency of 50 MHz.

3.2. Experimental Lamb waves

By assuming that the Young modulus, density, and Poisson's ratio of the aluminum specimen used in this study are 72000 MPa, 2700 kg/m³, and 0.33, respectively, the dispersion curves of the Lamb waves can be calculated by means of the Dispersion Calculator developed by the German Aerospace Center [25]. Since the central frequency 160 kHz is below the minimum frequencies for generating S_1 mode and A_1 mode Lamb waves, only S_0 and A_0 Lamb waves are observed in the experiment, and their group velocities at the frequency 160 kHz are 5.31×10^6 mm/s and 3.13×10^6 mm/s, respectively. The times of flight (ToF) of S_0 and A_0 waves can then be calculated by the velocities and the distance between the sensor and the actuator (140 mm), yielding 2.637×10^{-5} s and $4.473 \times$

Table 2

Calculation of future state and RUL at time step k .

Initialization: set $\{x_k^{i0} : i = 1, 2, \dots, N_p\}$ as $\{x_k^i : i = 1, 2, \dots, N_p\}$
For $i = 1 : N_p$
$j = 0$
While $x_k^{ij} < l_{th}$
Calculate the future state x_k^{ij+1} by $x_k^{ij+1} = f(x_k^{ij}, \theta_k^i)$
$j = j + 1$
End
$RUL_k^i = j \times \Delta N$
End

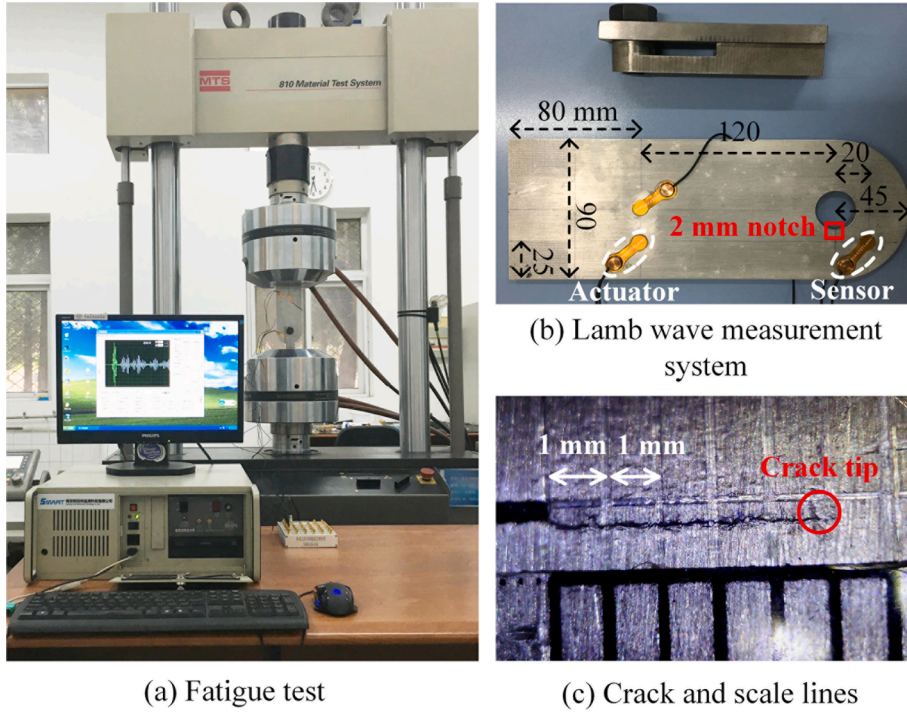


Fig. 2. Experimental setup.

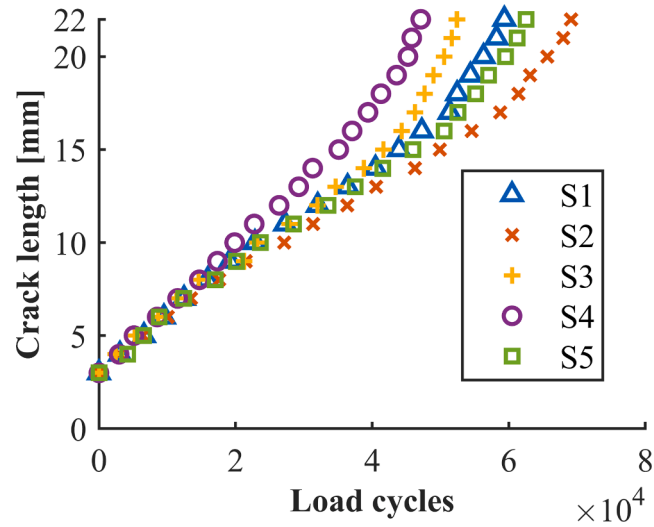


Fig. 3. Crack growths of specimens S1 ~ S5.

10^{-5} s, respectively.

Fig. 4 compares the analytical S_0 and A_0 arrivals with the experimental Lamb waves at three different crack lengths, over a time horizon of 1.2×10^{-4} s. The first wave package is a crosstalk caused by the electromagnetic induction between the circuits of the actuator and the sensor, so the start of the crosstalk (SoC) wave is approximately equivalent to the time at which the excitation from the actuator is applied to the structure [26]. The analytical arrivals of the S_0 and A_0 waves are approximately equal to the summation of the SoC and the S_0 wave ToF, and to that of the SoC and the A_0 ToF, respectively. A good match can be found between the calculated S_0 arrival and the start of the second wave package (i.e., the S_0 mode wave). The increasing crack lengths in general give rise to amplitude reductions of the S_0 waves, and consequently, to the variation of the feature extracted from these waves.

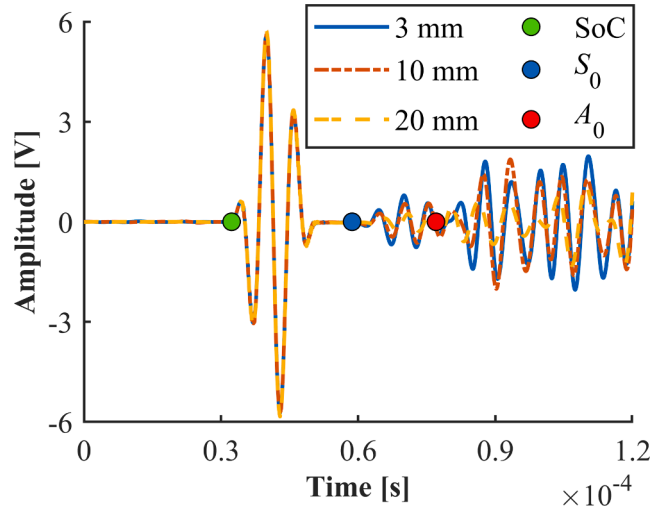


Fig. 4. Lamb wave signals at three crack lengths from specimen S1. Note: 'SoC' means 'start of crosstalk'.

3.3. Numerical Lamb waves

ABAQUS EXPLICIT is adopted to calculate the numerical S_0 Lamb waves of the aluminum lug structure at different crack lengths {3, 5, 8, 10, 12, 15, 18, 20, 22 mm}, as given in Fig. 5. Similarly to the case of Section 3.2, the Young's modulus, density, and Poisson's ratio of the aluminum used in this simulation are 72000 MPa, 2700 kg/m³, and 0.33, respectively. The structure and crack are modeled as '3D solid' and 'seam', respectively. The left side of the plate and the right side of the hole are fixed. The actuator and sensor are not modeled to save computation time. Two symmetric out-of-plane pressures are applied within the 4 mm radius (size of the actuator) circles on the two sides of the plate, whose amplitudes are shaped according to the 3-cycles Hanning-windowed sine burst, i.e., the same as the excitation used in the experiment. The out-of-plane displacements at the center of the sensor location are taken as the numerical Lamb wave of reference.

The mesh size of the finite element in a Lamb wave simulation, s_e , should satisfy [27]:

$$s_e < \frac{\lambda_{min}}{20} = 1.69 \text{ mm} \quad (9)$$

where the smallest wavelength λ_{min} is the S_0 mode wavelength 33.87 mm. Thus a mesh size of 1 mm used in this study is sufficiently small. As recommended by the ABAQUS user manual, the time step Δt for a stable simulation is determined according to:

$$\Delta t < \frac{L_{min}}{c_d} = 1.59 \times 10^{-7} \text{ s} \quad (10)$$

where the smallest element length L_{min} in the numerical model can be approximated as the mesh size (1 mm) and the longitudinal wave velocity is $c_d = 6.29 \times 10^6 \text{ mm/s}$. A step $\Delta t = 5 \times 10^{-9} \text{ s}$ is chosen in this study.

Fig. 6 shows the comparison between the initial times of the numerical S_0 mode Lamb waves at the three different crack lengths and the analytical S_0 arrival time. Similarly to the experimental Lamb waves in Fig. 4, the increasing crack lengths seem to give rise to a monotonic amplitude decrease of the numerical Lamb waves before $6 \times 10^{-5} \text{ s}$.

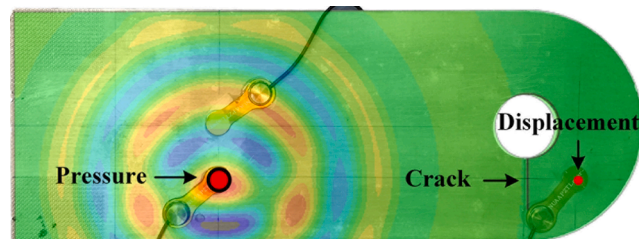


Fig. 5. Numerical setup.

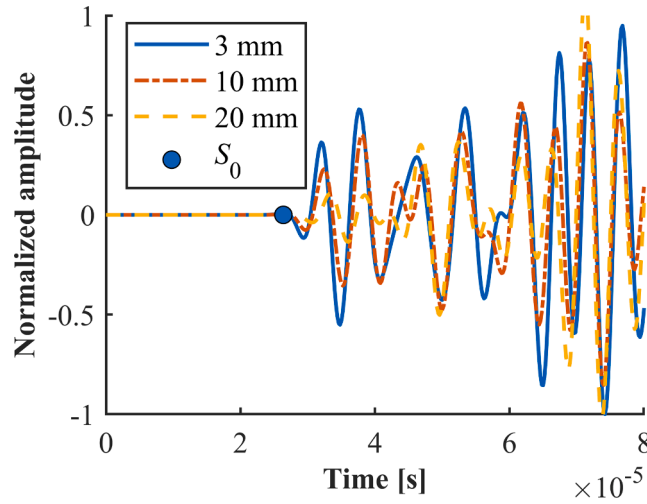


Fig. 6. Numerical S_0 mode Lamb waves and analytical S_0 arrival.

3.4. Comparison of numerical and experimental Lamb waves

Fig. 7 (a) and (b) show the comparisons of the numerical and experimental (specimen S1) Lamb waves at crack length 3 mm and 20 mm, respectively. The crosstalk of the experimental signal is replaced by zero values for simplicity. The numerical S_0 Lamb waves satisfactorily agree with the experimental ones before 4×10^{-5} s, similarly to the comparison of numerical and experimental Lamb waves shown in [16]. The differences showing up after the time 4×10^{-5} s might be due to multiple causes, for example, the differences between the simulated and the actual cracks, and those between the simulated and the actual excitation. An even more obvious difference can be noted after the A_0 arrival, as only the S_0 wave is numerically simulated, whereas both the S_0 and A_0 waves might co-exist in the experimental signals after the A_0 arrival.

3.5. Feature extraction

As already performed in [12,14], only the portion of the Lamb wave signals falling within a properly set time window are chosen for further processing, i.e., for extracting the statistical features for the estimation of the crack length. The window is defined to start at the S_0 arrival and with a width equal to 10^{-5} s.

The signal difference coefficient (SDC) [28] is chosen as the damage-sensitive statistical feature to be extracted from the Lamb waves, given its demonstrated performances in prognostic investigations [12,14]. It is defined as:

$$SDC_l = 1 - \left| \frac{cov(f_l, f_r)}{std(f_l)std(f_r)} \right| \quad (11)$$

where f_r and f_l are the windowed numerical Lamb waves at the initial crack length 3 mm and another generic crack length l mm, respectively, the function ‘cov’ is the covariance of the Lamb waves f_r and f_l , and the function ‘std’ is the standard deviation of an

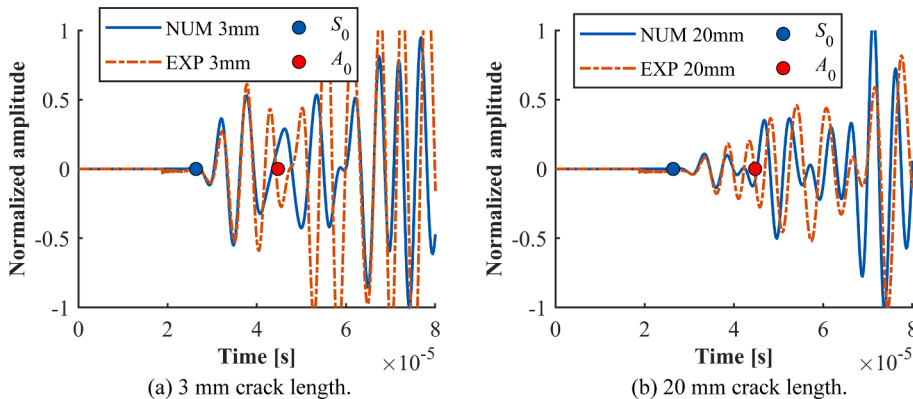


Fig. 7. Numerical and experimental (specimen S1) Lamb waves at two crack lengths.

individual set of signals. The same procedure is also carried out for the experimental Lamb waves from each of the available specimens.

The SDCs at different crack lengths from the numerical and experimental Lamb waves are given in Fig. 8, where a satisfactory match can be found between the two types of SDCs. The numerical SDCs at the nine crack lengths are used to build a 4-th order polynomial fitting regression function $g(\cdot)$ as:

$$g(x) = -2.3086 \times 10^{-5}x^4 + 1.2296 \times 10^{-3}x^3 - 0.0192x^2 + 0.1258x - 0.2477 \quad (12)$$

The crack growth data and the SDCs from specimen S1 will be processed in Section 4.2 for demonstrating the proposed framework, whereas the validation results using specimen S1 and the other specimens are given in Sections 4.3 and 4.4, respectively.

4. Validation of the proposed framework

Section 4.1 presents the state space model and the PF parameters. Section 4.2 illustrates the creation of a target crack growth and of the SDCs using the data of specimen S1. The feasibility and robustness of the proposed method are discussed in Sections 4.3 and 4.4, respectively.

4.1. State space model and PF parameters

The discretized Paris's law is adopted to describe the crack propagation as:

$$x_k = x_{k-1} + C(\Delta K(x_{k-1}))^m \Delta N \quad (13)$$

where x is the crack length, ΔN is the number of load cycles included in a discretization step, the two parameters C and m are the empirical values governing the crack growth, and ΔK is the stress intensity factor range as determined in the numerical simulations performed by some of the same authors in [14]:

$$\Delta K(x) = 0.0014x^3 + 0.5626x^2 - 13.50x + 497.8 \quad (14)$$

This strategy remains valid for more complex structures, where structural complexity may introduce more uncertainties like the unknown initial crack location or curved crack propagation. In this case, the ΔK may depend on multiple damage states, e.g., crack length, location, and shape, thus its calculation is similar to that in [14], but with more damage states involved.

The generic prognostic model of Eq. (4) can then be specified as:

$$\begin{cases} \mathbf{z}_k = \begin{bmatrix} \ln C_k \\ m_k \\ x_k \\ b_k \end{bmatrix} = \begin{bmatrix} \ln C_{k-1} + \omega_{1,k} \\ m_{k-1} + \omega_{2,k} \\ x_{k-1} + e^{\omega_k} C_k (\Delta K(x_{k-1}))^{m_k} \Delta N \\ b_{k-1} + \omega_{b,k} \end{bmatrix} \\ y_k = g(x_k) + b_k + \nu_k \end{cases} \quad (15)$$

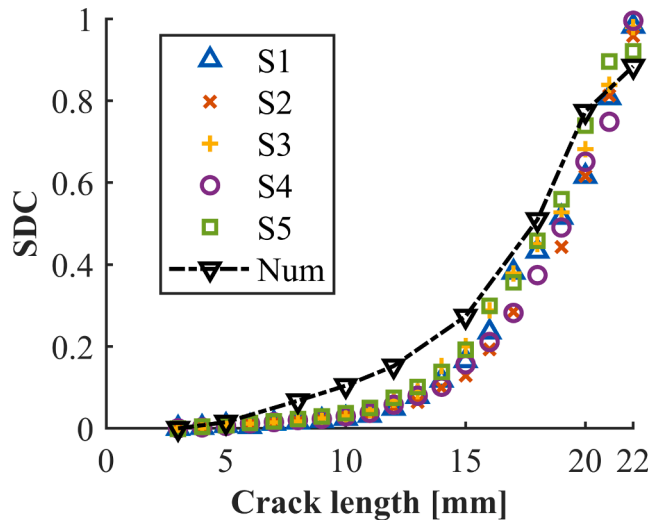


Fig. 8. SDCs at different crack lengths from numerical and experimental studies.

where $\omega \sim \mathcal{N}\left(-\frac{\sigma^2}{2}, \sigma^2\right)$ is the unbiased Gaussian process noise with standard deviation σ [1], ω_1 , ω_2 and ω_b are zero-mean Gaussian process noises and the measurement y is the feature SDC. Thus, Eq. (15) turns out to be a nonlinear and non-Gaussian model, due to the non-linearities of the Paris' law and the function $g(\cdot)$, and the non-Gaussian noise e^{ω} , respectively.

As the prognosis accuracy highly depends on the state estimation accuracy, one can resort to kernel smoothing [29] to improve the accuracy of estimating the time-invariant parameters $\ln C$ and m ,

$$\begin{cases} \ln C_k = \sqrt{1-h^2} \ln C_{k-1} + (1-\sqrt{1-h^2}) \widehat{\ln C}_{k-1} + \omega_{1,k} \\ m_k = \sqrt{1-h^2} m_{k-1} + (1-\sqrt{1-h^2}) \widehat{m}_{k-1} + \omega_{2,k} \end{cases} \quad (16)$$

where $h \in [0, 1]$ is the smoothing parameter, and $\widehat{\ln C}$ and \widehat{m} are the means of the samples for the parameters $\ln C$ and m , respectively.

Table 3 shows the values of the PF parameters used in this study, which are determined from [14] and by a trial-and-error procedure. The effects of these parameters on the PF performances can be found in [30] (number of particles), [11] (standard deviation of the measurement noise - likelihood function), [30] (process noise), and [30] (initial distribution or range).

4.2. Target crack growth and SDCs

The crack lengths and the Lamb waves in the experiment have been collected over a long-time interval (i.e., every several thousand load cycles). In order to simulate a realistic online SHM application scenario, where the Lamb waves can be collected at quite high frequencies (or, equivalently, at shorter load cycle intervals) for feature extraction, and consequently for crack length quantification, the crack growth and the SDCs from specimen S1 are used to create the target crack lengths and the corresponding experimental SDCs according to the following procedure [14]:

- Linearly interpolate the crack lengths from specimen S1 to generate a new target with more datapoints, where the crack lengths are available to measurements every 300 load cycles,
- Corrupt the crack lengths by white Gaussian noise with the signal-to-noise ratio (SNR) 50 dB to simulate stochasticity in the crack growth process,
- Use linear interpolation to generate a new SDC at each target crack length, and corrupt these SDCs by white Gaussian noise with SNR 30 dB to simulate the measurement noise.

Fig. 9 (a) shows the resulting target crack growth, where the number of load cycles is $N = 5.91 \times 10^4$. Fig. 9 (b) shows the target experimental SDCs (red dots) and the SDCs predicted by the function $g(\cdot)$ (dashed, grey line). A time-varying bias (blue dots) can be observed between the two types of SDCs, whose effects on the estimation of the crack length and the parameters $\ln C$ and m can be alleviated by adding a bias parameter into the state-space model for estimation as shown in Eq. (4) [14].

4.3. Estimation and prediction results

Fig. 10 (a) (b) and (c) present the estimates of the crack length, the parameters $\ln C$ and m , and the bias parameter b , respectively. As the bias between the measurements predicted by the function $g(\cdot)$ and the target measurements is satisfactorily identified, both the estimates of the posterior PDF of the crack length remain close to the target values, and the samples (particles) associated with the parameters $\ln C$ and m keep reducing their spread during the simulation and accumulate around some final values. On the other hand, the estimated bias turns out to be larger than the true one over the load cycle range between 3×10^4 and 5×10^4 , thus giving rise to estimated crack lengths smaller than the target ones in correspondence of the same load cycles (the opposite behavior can be observed after 5×10^4 load cycles).

The predicted future states at 3.6×10^4 load cycles are given in Fig. 11 (a), showing the estimated crack length (blue, dashed line), the crack length prediction trajectory (grey, dotted line), and the RUL posterior PDF (grey histogram). The predicted future states are well distributed around the true crack lengths due to the satisfactory estimation performances for the damage state and its propagation

Table 3
Particle filter parameters.

Number of particles N_p 8000	h in kernel smoothing 0.1	Standard deviation in likelihood function 0.01
Initial distributions for $\ln C$ [$\ln \frac{\text{mm}}{\text{cycle}(\text{MPa}\sqrt{\text{mm}})^{-m}]$, m [-]	Initial range for x [mm]	Initial value for b [-]
$\begin{bmatrix} \ln C_0 \\ m_0 \end{bmatrix} \sim \mathcal{N}\left(\begin{bmatrix} -57.18 \\ 8.101 \end{bmatrix}, \begin{bmatrix} 0.9966 & -0.1764 \\ -0.1764 & 0.0346 \end{bmatrix}\right)$	$x_0 \in (2.5, 3.5)$	$b_0 = 0$
Distributions of process noises $\{\omega, \omega_1, \omega_2, \omega_b\}$ for x , $\ln C$, m , b		
$\omega \sim \mathcal{N}\left(-\frac{0.01^2}{2}, 0.01^2\right)$	$\omega_1 \sim \mathcal{N}(0, 0.02^2)$	$\omega_2 \sim \mathcal{N}(0, 0.002^2)$ $\omega_b \sim \mathcal{N}(0, 0.01^2)$

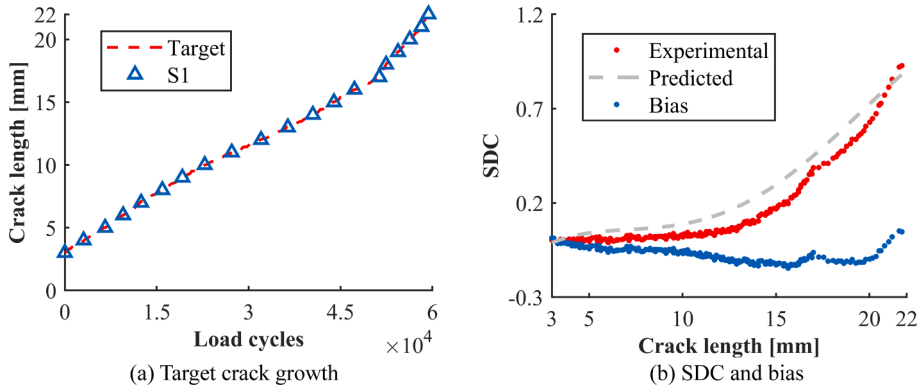


Fig. 9. Target crack growth, SDCs and bias.

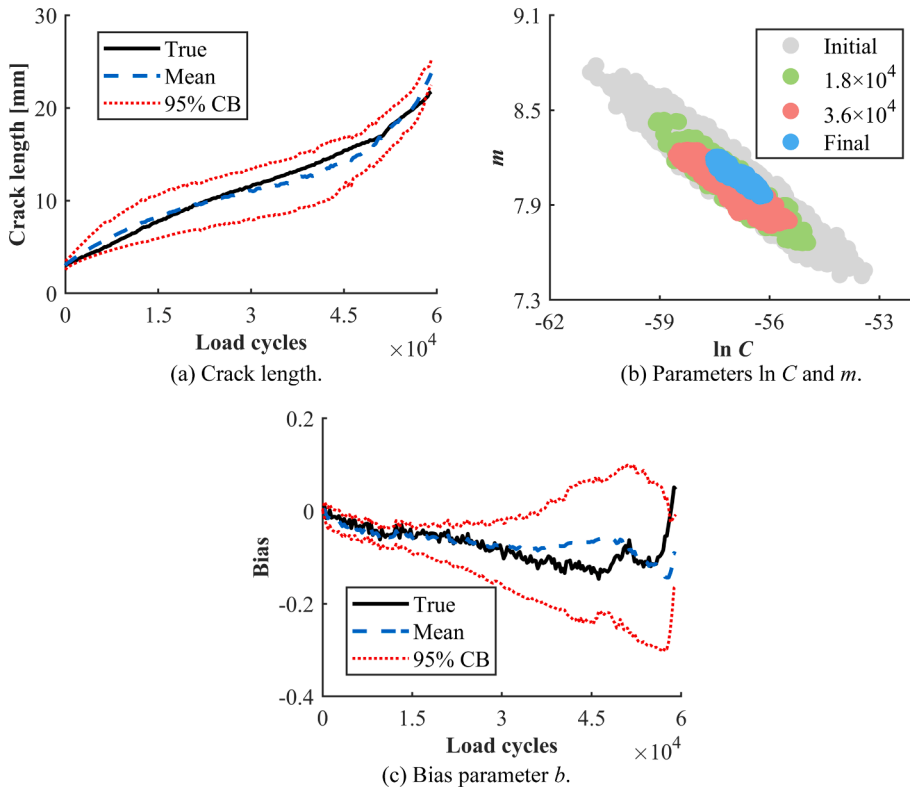


Fig. 10. Estimation for crack length, parameters $\ln C$ and m , and bias from specimen S1. Note: 'CB' means the confidence boundary.

parameters. This is also evident in the RUL prediction of Fig. 11 (b), where the predicted RUL is close to the target RUL, with confidence boundaries shrinking as the load cycles increase.

4.4. Validation with all specimens

The robustness of the proposed framework is now tested with the specimens S2 ~ S5. The procedure for creating the target crack growth and its corresponding SDCs for each specimen is the same as that for specimen S1. The analysis in Section 4.3 is repeated with the same PF parameters. Their crack length estimation and RUL prediction results are presented in Figs. 12 and 13, respectively, which can still yield the conclusions drawn from Fig. 10 (a) and 11(b), demonstrating the feasibility of the proposed method over different specimens. In fact, the method allows taking the uncertainties of both the damage evolution and the measurement models into account by simultaneously and online updating the damage evolution and the bias parameters. On the other hand, the performance of this method for each specimen is noted slightly different, which can hardly be avoided due to several reasons like the stochasticity in crack

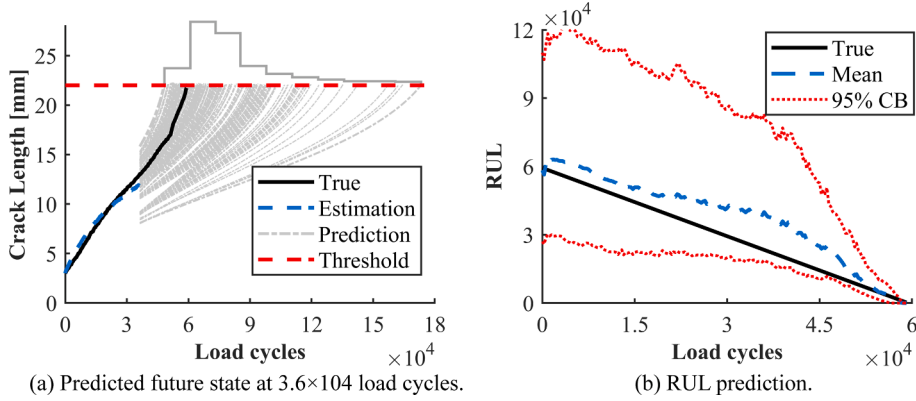


Fig. 11. Prediction for future crack length and RUL from specimen S1.

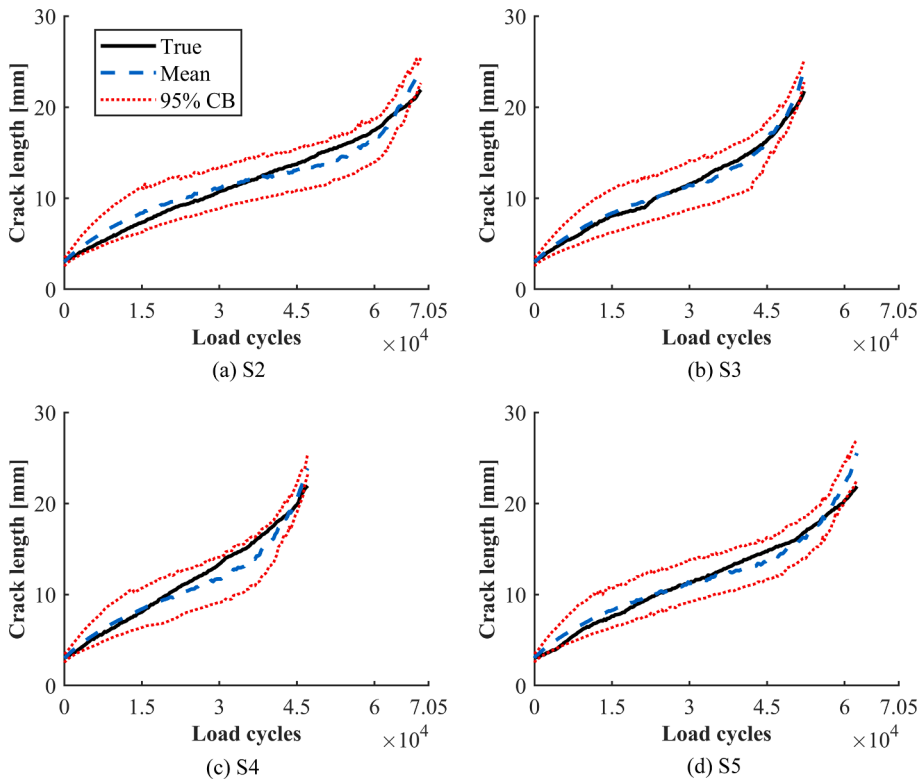


Fig. 12. Crack length estimation results from specimens S2 ~ S5.

growth and the magnitude of measurement bias.

The root-mean-square error (RMSE) of the crack length estimate, the cumulative relative accuracy (CRA) of the RUL, and the prognostic horizon (PH) of the RUL serve as the three metrics to evaluate the performances of the proposed method, i.e.:

$$RMSE = \sqrt{\frac{1}{T} \sum_{k=1}^T (\bar{x}_k - x_{true,k})^2} \quad (17)$$

$$CRA = \frac{1}{T-1} \sum_{k=1}^{T-1} \left(1 - \frac{|\overline{RUL}_k - RUL_{true,k}|}{RUL_{true,k}} \right) \quad (18)$$

where \bar{x} and \overline{RUL} denote the posterior estimates of the crack length and of the RUL, respectively, the subscript 'true' means the true

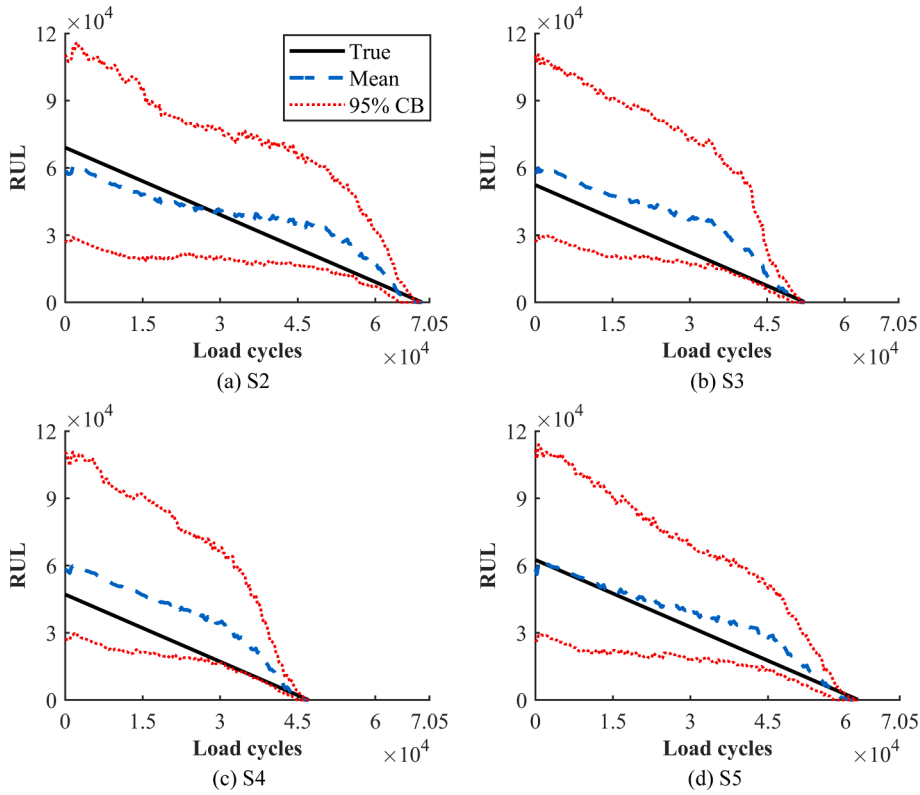


Fig. 13. RUL prediction results from specimens S2 ~ S5.

Table 4

Estimation and prognostic performances from all five specimens.

	S1	S2	S3	S4	S5
RMSE [mm]	0.709	0.911	0.578	1.039	0.866
CRA	0.628	0.678	0.486	0.365	0.727
PH [Load cycles]	9900	8400	7800	6300	11,400

crack length or RUL, T is the number of discrete load cycle steps required by the PF until failure is reached. Lower RMSE and higher CRA represent better estimation and prognosis performances, respectively.

PH is the difference between the current load cycle step and the end-of-prediction utilizing data accumulated up to the current step, provided the prediction meets desired specifications [31]. The end-of-prediction is the end of the test, i.e., the number of load cycles N , and the PH is the number of load cycles when 60% of the RUL distribution first falls within the range ‘true RUL $\pm 10\%N$ ’ [1].

Table 4 presents the RMSEs, CRAs, and PHs from all specimens, where the different performances of the proposed method over different specimens are more apparent. In order to further improve its robustness, one may refer to either (i) a PF with an adaptive process noise which enhances the performance in estimating the time-varying parameter [32], or (ii) the usage of multiple damage-sensitive features from Lamb waves to infer the unknown crack length [12].

5. Conclusions

Lamb wave-based damage prognosis methods typically require a data-driven measurement equation to describe the relationship between the damage state and some properly chosen damage-sensitive features of Lamb waves. The formulation of such a model generally requires sufficiently experimental or in-field datasets collected during the run-to-failure process, which, however, may not be available due to some causes like the high costs.

By combining a numerical simulation-aided damage quantification method with a damage prognosis framework accounting for the unavoidable measurement bias, this work has proposed a new particle filter-based damage prognosis framework, which only requires numerically simulated Lamb waves for building the measurement equation. The proposed framework has three advantages, i.e.,

- The costs and efforts in conducting run-to-failure tests and collecting experimental or in-field data for model formulation can be avoided.

- The numerical database developed in this work only consists of nine Lamb wave propagation simulations, each of which requires few computation efforts, i.e., about four minutes on an AMD Ryzen 9 3950X 16-Core Processor.
- The proposed method is robust, as validated by the results from the five specimens, because it takes the uncertainties from both the damage evolution and measurement models into account by online updating their parameters.

In a more realistic application scenario, where tens of or hundreds of sensors are installed for monitoring, the measurement vector in this method can be high-dimensional and most of the measurements far away from the damage can be damage-insensitive, which should possibly lead to an inaccurate and time-consuming prognosis. In order to deal with this problem, one may refer to a proper measurement partitioning strategy by online selecting limited-amount damage-sensitive measurements for estimation.

Declaration of Competing Interest

The authors declare that they have no known competing financial interests or personal relationships that could have appeared to influence the work reported in this paper.

Acknowledgments

This project has received funding from the European Union's Horizon 2020 research and innovation programme under the Marie Skłodowska-Curie grant agreement No. 859957.

References

- [1] M. Corbetta, C. Sbarufatti, M. Giglio, M.D. Todd, Optimization of nonlinear, non-Gaussian Bayesian filtering for diagnosis and prognosis of monotonic degradation processes, *Mech. Syst. Sig. Process.* 104 (2018) 305–322.
- [2] M. Corbetta, C. Sbarufatti, M. Giglio, A. Saxena, K. Goebel, A Bayesian framework for fatigue life prediction of composite laminates under co-existing matrix cracks and delamination, *Compos. Struct.* 187 (2018) 58–70.
- [3] M. Chiachio, J. Chiachio, S. Sankararaman, K. Goebel, J. Andrews, A new algorithm for prognostics using Subset Simulation, *Reliab. Eng. Syst. Saf.* 168 (2017) 189–199.
- [4] F. Cadini, C. Sbarufatti, M. Corbetta, F. Cancelliere, M. Giglio, Particle filtering-based adaptive training of neural networks for real-time structural damage diagnosis and prognosis, *Struct. Control Health Monit.* 26 (12) (2019).
- [5] N. Eleftheroglou, T. Loutas, Fatigue damage diagnostics and prognostics of composites utilizing structural health monitoring data and stochastic processes, *Struct. Health Monit.* 15 (2016) 473–488.
- [6] N. Eleftheroglou, D. Zarouchas, T. Loutas, R. Alderliesten, R. Benedictus, Structural health monitoring data fusion for in-situ life prognosis of composite structures, *Reliab. Eng. Syst. Saf.* 178 (2018) 40–54.
- [7] Y. Peng, M. Dong, M.J. Zuo, Current status of machine prognostics in condition-based maintenance: a review, *Int. J. Adv. Manuf. Technol.* 50 (1–4) (2010) 297–313.
- [8] L. Liao, F. Köttig, Review of Hybrid Prognostics Approaches for Remaining Useful Life Prediction of Engineered Systems, and an Application to Battery Life Prediction, *IEEE Trans. Reliab.* 63 (2014) 191–207.
- [9] P. Baraldi, F. Mangili, E. Zio, Investigation of uncertainty treatment capability of model-based and data-driven prognostic methods using simulated data, *Reliab. Eng. Syst. Saf.* 112 (2013) 94–108.
- [10] I. Lopez, N. Sarigul-Klijn, A review of uncertainty in flight vehicle structural damage monitoring, diagnosis and control: Challenges and opportunities, *Prog. Aerosp. Sci.* 46 (7) (2010) 247–273.
- [11] D. Cristiani, C. Sbarufatti, M. Giglio, Damage diagnosis and prognosis in composite double cantilever beam coupons by particle filtering and surrogate modelling, *Struct. Health Monit.* 1475921720960067 (2020).
- [12] J. Chen, S. Yuan, H. Wang, On-line updating Gaussian process measurement model for crack prognosis using the particle filter, *Mech. Syst. Sig. Process.* 140 (2020), 106646.
- [13] J. Chen, S. Yuan, X. Jin, On-line prognosis of fatigue cracking via a regularized particle filter and guided wave monitoring, *Mech. Syst. Sig. Process.* 131 (2019) 1–17.
- [14] T. Li, C. Sbarufatti, F. Cadini, J. Chen, S. Yuan, Particle filter-based hybrid damage prognosis considering measurement bias, *Struct. Control Health Monit.* 29 (4) (2022) e2914.
- [15] T. Stepinski, M. Mańka, A. Martowicz, Interdigital lamb wave transducers for applications in structural health monitoring, *NDT E Int.* 86 (2017) 199–210.
- [16] C. Sbarufatti, G. Manson, K. Worden, A numerically-enhanced machine learning approach to damage diagnosis using a Lamb wave sensing network, *J. Sound Vib.* 333 (2014) 4499–4525.
- [17] J. He, Y. Ran, B. Liu, J. Yang, X. Guan, A fatigue crack size evaluation method based on lamb wave simulation and limited experimental data, *Sensors* 17 (2017) 2097.
- [18] T. Peng, A. Saxena, K. Goebel, Y. Xiang, Y. Liu, Integrated experimental and numerical investigation for fatigue damage diagnosis in composite plates, *Struct. Health Monit.* 13 (2014) 537–547.
- [19] Y. Wu, X. Shen, D. Li, Numerical and experimental research on damage shape recognition of aluminum alloy plate based on Lamb wave, *J. Intell. Mater. Syst. Struct.* (2021), 1045389X21990885.
- [20] C.T. Ng, M. Veidt, A Lamb-wave-based technique for damage detection in composite laminates, *Smart Mater. Struct.* 18 (2009), 074006.
- [21] M.S. Arulampalam, S. Maskell, N. Gordon, T. Clapp, A tutorial on particle filters for online nonlinear/non-Gaussian Bayesian tracking, *IEEE Trans. Signal Process.* 50 (2002) 174–188.
- [22] A. Doucet, S. Godsill, C. Andrieu, On sequential Monte Carlo sampling methods for Bayesian filtering, *Stat. Comput.* 10 (2000) 197–208.
- [23] E. Zio, G. Peloni, Particle filtering prognostic estimation of the remaining useful life of nonlinear components, *Reliab. Eng. Syst. Saf.* 96 (2011) 403–409.
- [24] J. Chen, S. Yuan, L. Qiu, H. Wang, W. Yang, On-line prognosis of fatigue crack propagation based on Gaussian weight-mixture proposal particle filter, *Ultrasonics* 82 (2018) 134–144.
- [25] https://www.dlr.de/zlp/en/desktopdefault.aspx/tabid-14332/24874%7B/_%7Dread-61142/%7B/24874_read-61142/.
- [26] L. Qiu, S. Yuan, X. Shi, T. Huang, Design of piezoelectric transducer layer with electromagnetic shielding and high connection reliability, *Smart Mater. Struct.* 21 (2012), 075032.
- [27] F. Moser, L.J. Jacobs, J. Qu, Modeling elastic wave propagation in waveguides with the finite element method, *NDT E Int.* 32 (1999) 225–234.
- [28] X.P. Qing, H.-L. Chan, S.J. Beard, A. Kumar, An Active Diagnostic System for Structural Health Monitoring of Rocket Engines, *J. Intell. Mater. Syst. Struct.* 17 (2006) 619–628.

- [29] J. Liu, M. West, Combined parameter and state estimation in simulation-based filtering, Sequential Monte Carlo methods in practice, in: A. Doucet, N. Freitas, N. Gordon (Eds.), Sequential Monte Carlo Methods in Practice, Springer New York, New York, NY, 2001, pp. 197–223.
- [30] E.N. Chatzi, A.W. Smyth, The unscented Kalman filter and particle filter methods for nonlinear structural system identification with non-collocated heterogeneous sensing, Struct. Control Health Monit. 16 (2010) 99–123.
- [31] A. Saxena, J. Celaya, E. Balaban, K. Goebel, B. Saha, S. Saha, M. Schwabacher, Metrics for evaluating performance of prognostic techniques, in: International Conference on Prognostics and Health Management, 2008, pp. 1–17.
- [32] M. Liu, S. Zang, D. Zhou, Fast leak detection and location of gas pipelines based on an adaptive particle filter, Int. J. Appl. Math. Comput. Sci. 15 (2005) 541–550.